Rotavirus mRNAS are released by transcript-specific channels in the double-layered viral capsid

Javier Periz[a], Cristina Celma[b], Bo Jing[a], Justin N. M. Pinkney[a], Polly Roy[b,1], and Achillefs N. Kapanidis[a,1]

[a]Biological Physics Research Group, Clarendon Laboratory, Department of Physics, University of Oxford, Oxford OX1 3PU, United Kingdom; and [b]Department of Pathogen Molecular Biology, Faculty of Infectious and Tropical Diseases, London School of Hygiene and Tropical Medicine, London WC1E 7HT, United Kingdom

Edited by Peter Palese, Mount Sinai School of Medicine, New York, NY, and approved June 10, 2013 (received for review December 2, 2012)

Rotaviruses are the single most common cause of fatal and severe childhood diarrheal illness worldwide (>125 million cases annually). Rotavirus shares structural and functional features with many viruses, such as the presence of segmented double-stranded RNA genomes selectively and tightly packed with a conserved number of transcription complexes in icosahedral capsids. Nascent transcripts exit the capsid through 12 channels, but it is unknown whether these channels specialize in specific transcripts or simply act as general exit conduits; a detailed description of this process is needed for understanding viral replication and genomic organization. To this end, we developed a single molecule assay for capturing and identifying transcripts extruded from transcriptionally active viral particles. Our findings support a model in which each channel specializes in extruding transcripts of a specific segment that in turn is linked to a single transcription complex. Our approach can be extended to study other viruses and transcription systems.

channel specialization | Reoviridae | single molecule hybridization | single-stranded RNA

Double-stranded RNA (dsRNA) viruses comprise a wide variety of families that vary in genome complexity. These families include Reoviridae with 10–12 genomic segments; Crysoviridae with 4 segments; Cystoviridae with 3 segments; Birnaviridae, Picobirnaviridae, and Partiviridae with 2 segments; and Totiviridae with a single genomic dsRNA. They also vary in their ability to infect diverse hosts from bacteria to humans, yet they share unique features reflecting parallels in their replication; for the Reoviridae, such features include a multicomponent capsid that crosses the host cell membrane and transcription of their dsRNA segments by capsid-attached enzymes. During cell entry, the outer layers of these viruses are lost, while their inner capsids provide a compartment for genome segments (10-12 dsRNAs). Transcript export occurs via channels at the 12 vertices of an icosahedral capsid; although crucial for establishing infection (because the transcripts act as templates for both translation and genomic dsRNA synthesis), the mechanism of transcript export is unclear. In particular, it is unknown whether the nascent transcripts are selectively released through specialized channels, and if so, what the basis of selectivity is.

To address these questions, we studied rotavirus, a major cause of gastroenteritis in infants and children worldwide (1, 2), and a member of the Reoviridae family, which includes many viruses of veterinary and biomedical importance (3). Rotaviruses deliver a 70-nm-diameter double-layered particle (DLP) to host cells following entry; the outer and inner protein layers package transcription complexes (TCs), proteins VP1 (RNA-dependent RNA polymerase) and VP3 (RNA capping enzyme), and 11 dsRNA genomic segments. The outer DLP layer is made of VP6 proteins (4) arranged as pentamers and hexamers forming 132 channels of three classes, including a class of 12 channels, each placed at the fivefold vertices of the icosahedral capsid. Underneath the VP6 layer is the single-layered particle, which comprises VP2 proteins and forms a thin continuous scaffolding layer, except for small pores along the fivefold axis of the icosahedron. These pores are in register with the 12 VP6 channels and serve as RNA exit channels for the newly transcribed positive sense single-stranded RNA (ssRNA). Close to these channels, 12 TCs interact with the viral genomic segments and attach to a hub-like structure formed by VP2 (5, 6). This organization implies that 1 of the 12 TCs could be unoccupied (7–9).

Rotavirus RNA synthesis is thought to be asynchronous and moderately fast [50 nt/s for related orthoreovirus (10)], with some transcripts produced earlier than others (11). It has also been shown that transcripts are released simultaneously through the 12 RNA exit channels (12), but the assignment of specific segments to channels (if any) is unknown, because standard microscopy can only visualize the presence, but not the identity, of the extruded segments per single particle.

The DLP structural organization is compatible with two mechanistic models for transcript extrusion (Fig. 1). The channel specialization model (Fig. 1*A*) postulates that each channel is linked to a specific TC and to transcripts of only one specific genomic segment (13); this model predicts that, at any given time, only one transcript of a specific segment can be extruded per channel of a DLP. In contrast, the channel generality model (Fig. 1*B*) predicts that each channel can extrude transcripts of multiple (perhaps all) genomic segments, but only one at a time. This model also predicts that, at any given time, a genomic segment may interact with several TCs; thus, some particles carry two or more transcripts of a specific segment extruded from two or more channels. Hybrid versions of the two main models are also possible.

To test these models, we determined the copy number of specific transcripts during their extrusion from transcriptionally active DLPs using a novel single-molecule fluorescence assay for transcript capture and identification (hereafter, CID assay; Fig. 2). CID combines RNA hybridization with single-molecule imaging using alternating-laser excitation (14, 15) on a total internal reflection microscope (TIRF) (16). CID has the advantage of maintaining the transcriptional activity of viral particles, in contrast to approaches that may induce conformational changes in the channels, such as the use of anchor antibodies (17, 18) or labeling methods that target surface amines or cysteines. Our findings support the channel specialization model and exclude alternative models in which an individual segment is transcribed by several complexes and extruded through multiple channels. Our method can be implemented in the sensing of transcripts in other biological model systems.

Author contributions: J.P., P.R., and A.N.K. designed research; J.P., C.C., and J.N.M.P. performed research; J.P., B.J., and J.N.M.P. analyzed data; and J.P., P.R., and A.N.K. wrote the paper.

The authors declare no conflict of interest.

This article is a PNAS Direct Submission.

Freely available online through the PNAS open access option.

[1]To whom correspondence may be addressed. E-mail: Polly.Roy@lshtm.ac.uk or a.kapanidis1@physics.ox.ac.uk.

This article contains supporting information online at www.pnas.org/lookup/suppl/doi:10.1073/pnas.1220345110/-/DCSupplemental.

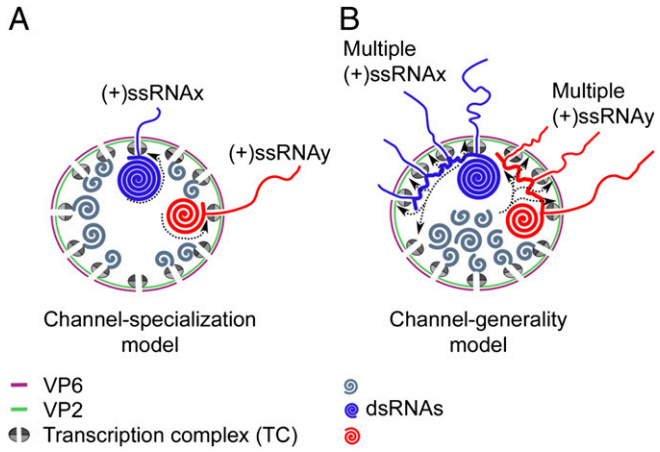

Fig. 1. Models for transcript exit in rotavirus. (*A*) Channel specialization model: each RNA exit channel is linked to a specific TC and transcripts (thin blue and red lines for *segments x and y*, respectively) of a single specific genomic segment (thick blue and red lines for *segments x and y*, respectively). This model predicts that only a single transcript of each viral genomic segment is extruded from each DLP at any given time. (*B*) Channel generality model: a segment can interact with multiple TCs and their corresponding RNA exit channels during transcription. This model predicts that multiple transcripts from each genomic segment can be extruded from each DLP at any given time.

Results

RNA Identification Assay Based on Single-Molecule Hybridization. CID uses three ssDNA probes complementary to sequences close to the 5′ end of a specific transcript: a biotinylated DNA for capturing RNAs on neutravidin-coated surfaces (capture probe C) and two fluorescent DNAs for identifying specific RNAs. The fluorescent DNAs were each labeled using a spectrally distinct fluorophore, with the two fluorophores serving as a donor–acceptor pair for Förster resonance energy transfer (FRET); we refer to these DNA probes as the green (G) and red (R) FRET probes (Fig. 2*A*). The fluorophore positions were chosen to ensure that target hybridization results in a specific combination of FRET efficiency and stoichiometry, hereafter termed an E^*/S code. In most experiments, we used a 0.35/0.5 E^*/S code; i.e., a single fully hybridized transcript led to FRET efficiency of 35% ($E^* \sim 0.35$) and relative probe stoichiometry S of 0.5 (corresponding to a 1:1 donor:acceptor hybrid; see *SI Materials and Methods*). The probe sequences were varied to target different transcripts (Table S1).

To establish that CID identifies transcripts with high sensitivity and specificity, we targeted a synthetic RNA version of the *segment 11* transcript using capture probe C_{11} and FRET probes G_{11} and R_{11} (Fig. 2*B*; *SI Materials and Methods*). After hybridization, surface capture, and single-molecule imaging, the E^*/S histograms showed a single population of molecules with the designed code of 0.35/0.5 (Fig. 2*B*). Further experiments to capture synthesized ssRNA11 from RNA transcribed from DLPs also showed the specific E^*/S code (Fig. S1).

These results matched exactly those for a positive control, a dsDNA construct (T_{11}-G_{11}-R_{11}) wherein the ssRNA11-specific FRET probes hybridize to a complementary biotinylated DNA (T_{11}) to produce the 0.35/0.5 code (Fig. 2*C*). As a negative control, we tested for any nonspecific binding of the transcript from *segment 11* to a probe set (G_6, R_6, and C_6) complementary to a transcript from *segment 6*; only two particles were captured, and none with the correct code (Fig. 2*D*).

We then tested whether CID can detect both extruded and released rotavirus transcripts from transcriptionally active DLPs (11, 13, 19) by monitoring ssRNA6 synthesis after adding nucleotides in mixtures of DLPs carrying probes specific for *segment 6* (G_6, R_6, and C_6). After allowing 2 min of transcription, transcripts were hybridized for up to 60 min (Fig. 2*E*), captured, and imaged. After hybridization for 15 min, ssRNA6 transcripts were clearly visible, matching the positive control (T_6-G_6-R_6; Fig. 2*F*); the number of detected transcripts increased with hybridization time. All populations had S values of ~0.5, showing that transcripts do not self-associate to higher-order structures on their release from DLPs; there was also no probe self-association (Fig. 2*G*). These results showed a high level of transcription from DLPs even for short incubations with nucleotides.

Capture of Extruded Transcripts from DLPs Using CID. Subsequently, we detected specific transcripts during their extrusion from DLPs (and before their release) by capturing DLPs with transcripts of *segments 6 and 11* extruded simultaneously (Fig. 3). To detect such DLPs, we allowed transcription for 1 min (*SI Materials and Methods*), during which DLPs should produce 10–20 transcripts of each segment [assuming transcription at ~50 nt/s (9)], with one transcript still attached to a DLP. After fixing the transcribing DLPs (*SI Materials and Methods*), we hybridized them to an ssRNA6 capture probe and ssRNA11 FRET probes; captured DLPs (311 particles) showed the expected code for a DLP carrying ssRNA11 transcripts (Fig. 3*A*) and exactly matched the code of the positive control (T_{11}-G_{11}-R_{11} construct; Fig. 3*B*). In a negative control (no nucleotides; Fig. 3*C*), we captured only four molecules, and none with the code. These results showed that DLPs were captured through an extruded ssRNA6 transcript while carrying a yet undetermined number of extruded transcripts of *segment 11*. However, the S value of ~0.5 for the main population and the absence of other populations of hybridized particles on the E^*/S histogram (Fig. 3*A*) excluded relative stoichiometries of the two FRET probes other than 1:1 and further suggested the presence of only a single extruded ssRNA11 per DLP. For example, if a significant number of DLPs carried two extruded ssRNA11 transcripts, the bleaching or substoichiometric hybridization for some particles would have resulted in populations with 2:1 or 1:2 G:R stoichiometry and in broadening of the S distribution relative to the 1:1 positive control (Fig. S2). In contrast, the S distribution for the captured DLPs matches exactly that of the 1:1 positive control (cf. black distributions in Fig. 3 *A* and *B*).

To confirm the presence of a single extruded transcript of ssRNA11 per DLP, we compared the DLP-based acceptor emission intensity on acceptor excitation ($A_{ex}A_{em}$, a FRET-independent measure of the number of acceptor fluorophores per particle; using data from Fig. 3*A*) with that of the positive control (T_{11}-G_{11}-R_{11} construct, with an absolute G:R stoichiometry of 1:1; Fig. 3*B*). For a single extruded transcript per DLP, the mean $A_{ex}A_{em}$ intensity for the captured DLPs should match that of the 1:1 control; however, if the DLPs carry two (or more) extruded transcripts for ssRNA11, the mean $A_{ex}A_{em}$ for DLPs should be twofold higher (or more) than that of the 1:1 control (see Fig. S2 *C* and *G* for the $A_{ex}A_{em}$ distribution for standards with G:R stoichiometries of 1:1 and 1:2, respectively; also see Fig. S2*J* for the mean $A_{ex}A_{em}$ of the same standards). Our results showed no differences between the mean $A_{ex}A_{em}$ intensity per captured DLP and the control (Fig. 3*D*; 5,492 ± 84 counts for DLPs; 5,673 ± 65 for the 1:1 control), leading us to conclude that only a single ssRNA11 transcript was present on the surface of each DLP during transcription.

To examine whether the extrusion of a single transcript per segment on transcribing DLPs applied to other segments, we targeted DLPs by swapping the capture and FRET probes used previously (i.e., we used a capture probe for ssRNA11 and FRET probes for ssRNA6). We performed the hybridization under the same conditions as those carried out to capture ssRNA6. To

MICROBIOLOGY

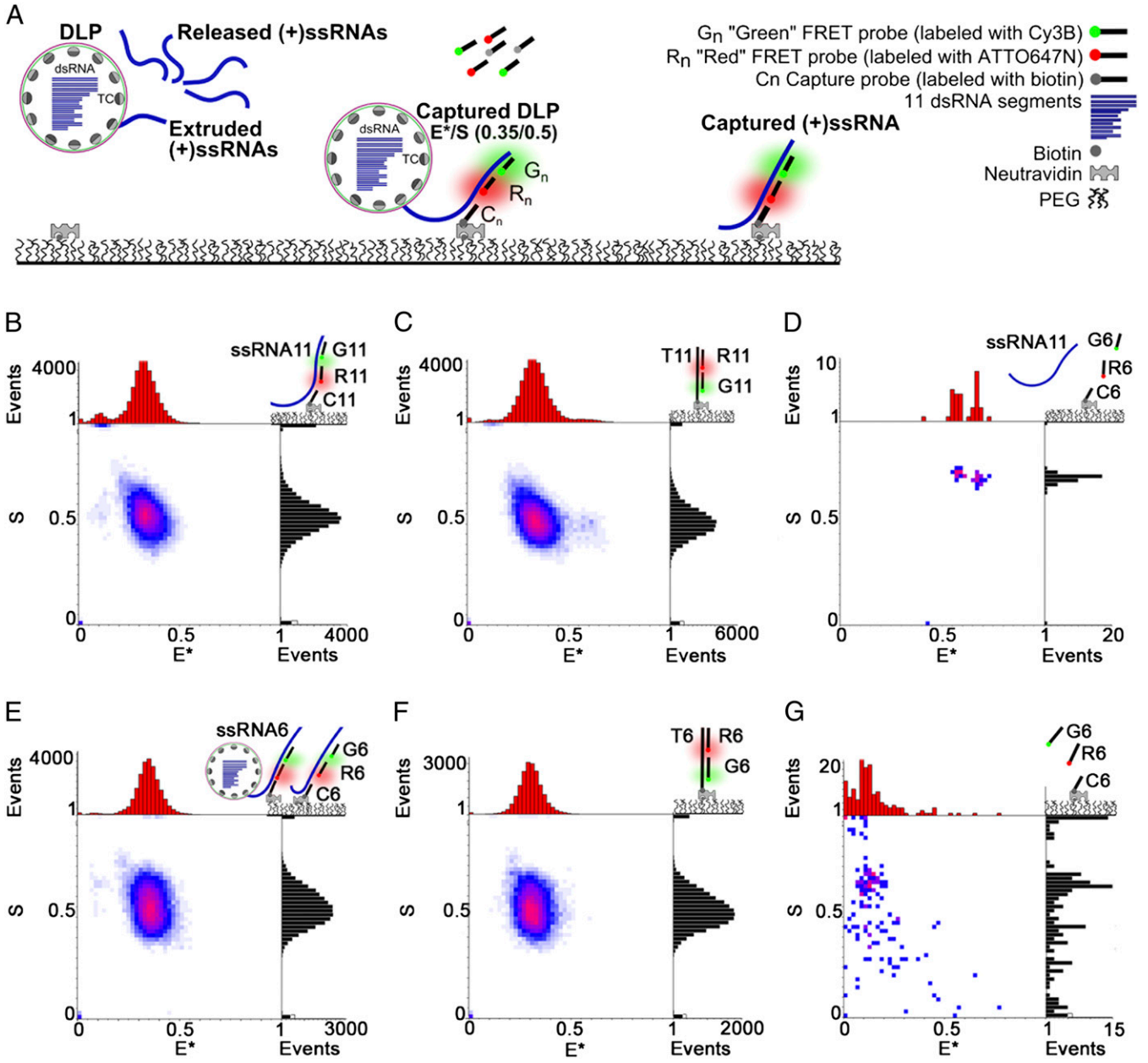

Fig. 2. CID detects specific transcripts from transcriptionally active viral particles. (*A*) Schematic of the CID assay. Transcripts (either attached to DLPs or free) are incubated with complementary capture and FRET probes (donor shown in green; acceptor shown in red), captured to the surface and detected using ALEX-TIRF. Specific transcripts are linked to specific combinations ("codes") of FRET efficiency *E** and relative probe stoichiometry *S*; in most cases, an *E*/S* code of 0.35/0.5 is used. (*B*) The synthetic (+)ssRNA11 using FRET probes (G_{11} and R_{11}) and capture probe C_{11} (hybridization strategy, top right) gives a 2D *E*/S* histogram (n = 1,895 particles) with the expected *E*/S* code. (*C*) Positive control using T_{11}-G_{11}-R_{11}, a dsDNA construct made of G_{11} and R_{11} hybridized to a complementary biotinylated ssDNA (T_{11}) matching a sequence in (+)ssRNA11. The *E*/S* histogram (n = 2,043) shows the *E*/S* code of 0.35/0.5. (*D*) Negative control does not show a specific signal when incubating (+)ssRNA11 with FRET probes G_6, R_6 and capture probe C_6 targeting (+)ssRNA6. (*E*) Detection of nascent (+)ssRNA6 transcripts from transcriptionally active DLPs, either while extruded from DLPs or after their release. DLP transcription was allowed to proceed for 2 min in the presence of G_6, R_6, and C_6. *E*/S* histograms (n = 1,402) clearly show the expected code after 60 min of hybridization. (*F*) Positive control using construct T_6-G_6-R_6 (designed as in *B*); the *E*/S* code for the control matches the signature for transcripts in *E*. (*G*) Negative control does not show a specific signal when incubating probes G_6, R_6, and C_6 in the absence of (+)ssRNA6.

improve DLP capture, we used an additional capture probe (C_{10}) targeting ssRNA10; the results also showed the same ssRNA6-specific signal (Fig. 3*E;* 322 particles). The presence of a single capture probe (C_{11}) under these hybridization conditions resulted in a specific signal but less efficient capture of transcripts (38 particles; Fig. S3). The signal specificity was supported by comparisons with the positive control (matching the signal for released ssRNA6; Fig. 3*F*; 1,832 particles) and the negative control (8 particles showing no specific signal without capture probes; Fig. 3*G*). Finally, as with ssRNA11 (Fig. 3*H*), the mean $A_{ex}A_{em}$ intensity for probe R_6 hybridized in DLPs matched that of the positive control (3,915 ± 72 counts for DLPs; 4,000 ± 37 for the 1:1 control), suggesting that the captured DLPs carry only a single extruded ssRNA6 transcript. Additional experiments aimed at the detection of a third rotavirus segment (ssRNA2) also showed the extrusion of a single transcript (Fig. S4).

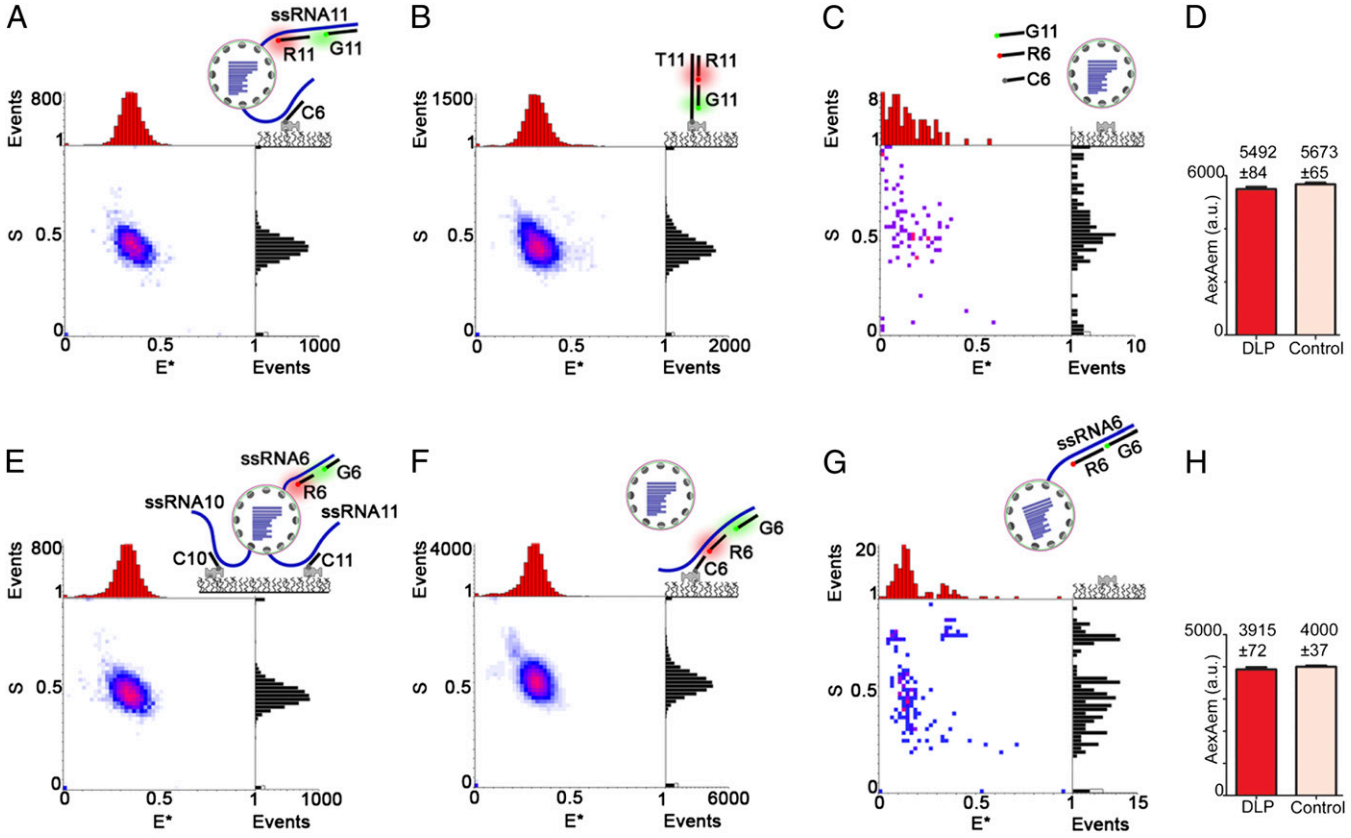

Fig. 3. Transcriptionally active DLPs carry a single extruded transcript for *segments 6 and 11*. (*A*) CID of actively transcribing DLPs (allowed to transcribe for 2 min) interrogated using probe C_6 [which targets extruded (+)ssRNA6] and probes G_{11} and R_{11} [which target extruded (+)ssRNA11]. The *E*/S* histogram (n = 311) shows an *E*/S* population of 0.35/0.5, matching that of the positive control (*B*). (*B*) Positive control. The *E*/S* histogram (n = 640) for construct T_{11}-G_{11}-R_{11} (Fig. 2*C*) shows the expected *E*/S* code of 0.35/0.5. (*C*) Negative control. *E*/S* histogram (n = 4) from DLPs incubated under the same experimental conditions but without nucleotides shows no specific signal. (*D*) Comparison of $A_{ex}A_{em}$ fluorescence intensities (mean ± SEM from experiments in *A* and *B*). Hybridized DLPs, red bar; positive control using T_{11}-G_{11}-R_{11}, pink bar. A *t*-test comparison between the results shows no significant differences in the mean ($P > 0.10$). (*E*) CID of actively transcribing DLPs (allowed to transcribe for 2 min) interrogated using probes C_{10} and C_{11} [which target extruded (+)ssRNA10 and (+)ssRNA11, respectively] and probes G_6 and R_6 [which target extruded (+)ssRNA6]. The *E*/S* histogram (n = 322) shows an *E*/S* population of 0.35/0.5, matching that of the positive control (*F*). (*F*) Positive control. The *E*/S* histogram (n = 1,832) for captured (+)ssRNA6 (synthesized under the same conditions as in *E* and detected using C_6, G_6, and R_6) shows the expected *E*/S* code of 0.35/0.5. (*G*) Negative control performed with FRET probes but in the absence of a capture probe do not show any specific hybridization (n = 8). (*H*) Comparison of $A_{ex}A_{em}$ fluorescence intensities (mean ± SEM from experiments in *E* and *F*). Hybridized DLPs, red bar; positive control using (+)ssRNA6, pink bar. A *t*-test comparison between the results shows no significant differences in the mean ($P > 0.35$).

These results establish that, for *segments 2, 6, and 11*, at most one single transcript of each of these rotavirus genes is being extruded from a DLP at any given time, and argue for a general mechanism in which at most one single transcript of any segment is synthesized and released from a DLP at any given time.

To confirm that the detected ssRNAs colocalize with DLPs, we performed CID experiments using antibodies for DLP capture (Fig. 4) instead of DNA capture probes. Specifically, we captured transcribing DLPs using a sheep antibody targeting VP6 (the protein covering the DLP surface with 780 copies) and a rabbit biotinylated antibody against sheep IgG; the DLPs were probed for the presence of extruded ssRNA2 (Fig. 4*A*). The *E*/S* histogram for the captured DLPs (Fig. 4*B*) displays a single population (n = 120) with the ssRNA2-specific *E*/S* code of ~0.35/0.5, thus matching the results for DLPs captured using DNA-based capture probes (Fig. S4). This single population matches the *E*/S* populations in two positive controls: probed ssRNA2 released from DLPs (Fig. 4*C*) and probed synthetic ssRNA2 (Fig. 4*D*), both captured using the C2 probe. Furthermore, the mean $A_{ex}A_{em}$ intensity for probe R_2 hybridized on antibody-captured DLPs matches those of the positive controls (Fig. 4*E*), showing that only a single ssRNA2 is being extruded from a DLP at a given time.

We also performed two negative controls. First, we substituted the VP6-specific antibody with rabbit γ-globulins and found only 12 colocalizations (some with the right code, possibly due to nonspecific interactions between DLPs and γ-globulins). Second, we performed immune-capture in the absence of the biotinylated secondary antibody; this pulled down only one particle and it did not have the correct *E*/S* code. These results confirmed that the vast majority of probed ssRNA molecules are attached to transcriptionally active surface-captured DLPs.

Actively Transcribing DLPs Carry Single Extruded Transcripts of *Segments 6 and 11*. To confirm that specific transcripts are extruded through single channels, we modified our CID assay to directly observe colocalization of ssRNA6 and ssRNA11 transcripts at the single DLP level (Fig. S5). This modification was achieved by using an ssRNA6-specific probe pair (capture probe C_6 and reporter probe G_6) and an ssRNA11-specific probe pair (capture probe C_{11} and reporter probe R_{11}). If our predictions were correct, the probing of actively transcribing DLPs using these four probes should capture particles with an *E*/S* value of 0.1/0.5, because independent transcripts extruded through

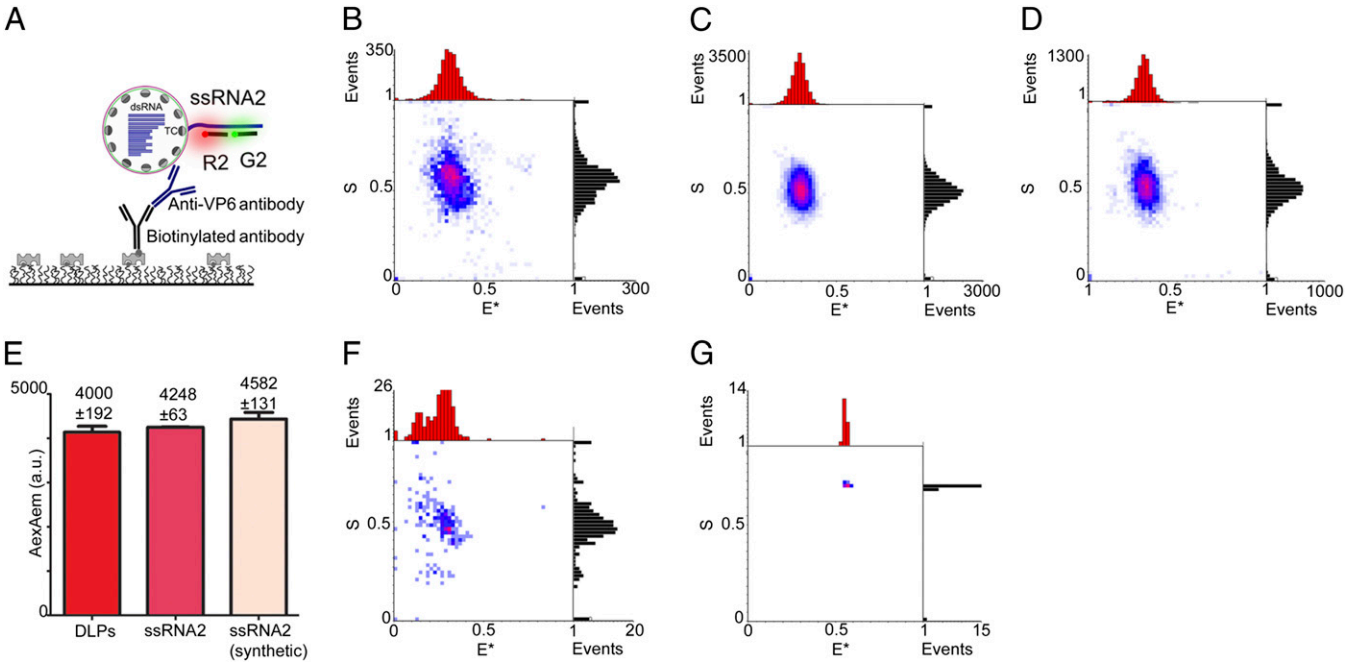

Fig. 4. Antibody-captured transcriptionally active DLPs carry a single extruded transcript for *segment 2*. (*A*) Schematic of the antibody-based CID assay. Actively transcribing DLPs (allowed to transcribe for 2 min) were interrogated using FRET probes G_2 and R_2 [which target (+)ssRNA2]. After incubation with a VP6-specific sheep antibody, the DLPs were added to a coverslip coated with a biotinylated rabbit anti-sheep antibody. For details, see *SI Materials and Methods*. (*B*) CID of antibody-captured actively transcribing DLPs interrogated using probes G_2 and R_2. The *E*/S* histogram (n = 120) shows a single *E*/S* population of 0.35/0.5, matching the main populations of the positive controls (*C* and *D*). (*C*) Positive control. The *E*/S* histogram (n = 879) for (+)ssRNA2 transcripts captured from transcribing DLPs using FRET probes R_2, G_2 and capture probe C_2 shows a single *E*/S* population of 0.35/0.5. (*D*) Positive control. The *E*/S* histogram (n = 414) for synthetic (+)ssRNA2 transcripts captured using the same probes as in *C* shows a single *E*/S* population of 0.35/0.5. (*E*) Pairwise comparison of the $A_{ex}A_{em}$ fluorescence intensities (mean ± SEM) from experiments in *B* (red bar), *C* (dark pink bar), and *D* (light pink bar). A one-way ANOVA using a Tukey's test shows no significant differences between DLPs and the ssRNA control ($P > 0.05$), supporting that only one ssRNA2 is extruded from the DLP at any given time. (*F*) Negative control. A CID assay performed as in *A* and *B*, but with the primary antibody being substituted by rabbit IgG (which does not bind to VP6). The *E*/S* histogram shows only few particles (n = 12) with an *E*/S* population of 0.35/0.5. (*G*) Negative control. A CID assay performed as in *A* and *B* but in the absence of a secondary antibody. Only a single particle is detected on the surface.

independent channels should be beyond FRET range (>10 nm; the E^* of ~0.1 is due to cross-talk between emission channels; *SI Materials and Methods*). Indeed, the DLP sample (357 particles) showed E^*/S values of ~0.1/0.5 (Fig. S5*A*). Due to the nature of the sample (which contains both DLPs with extruded RNAs and released RNAs), the colocalization is in part due to captured DLPs and in part due to random coincidence of released transcripts. The degree of ssRNA6–ssRNA11 colocalization for the DLP sample was higher (P = 0.0004; Fig. S5*B*) than what was expected on the basis of random coincidence (*SI Materials and Methods*), supporting the presence of significant specific transcript colocalization on the captured DLPs. These colocalization experiments provided an opportunity to test the hypothesis that rotavirus transcripts can associate independently and guide sequence assortment during encapsidation (7). We thus used our CID assay to test for such an association between ssRNA6 and ssRNA11. We synthesized all transcripts (preparing a "total ssRNA" sample) by DLP transcription, followed by DLP removal (Fig. S5*B*). The number of colocalizations for total ssRNA was then compared with the colocalizations expected due to random coincidence; the absence of any statistically significant difference further supported that the DLP-dependent colocalisation arises due to specific colocalization of transcripts on DLPs as opposed to colocalization due to capture of higher-order complexes of transcripts; we also conclude that, under our conditions, there is no detectable direct or indirect (within a higher-order self-assembled structure) association of ssRNA6 and ssRNA11.

Discussion

In this study, we introduce a CID assay for studying the synthesis of specific transcripts from rotavirus particles. The assay has a simple design and allows unambiguous identification and quantification of specific ssRNAs. We implemented the CID assay to study the extrusion and release of specific transcripts from rotavirus particles and characterized the specialization of the transcript exit channels for two specific segments.

CID Assay. The assay is based on a coding strategy that relies on two single-molecule fluorescence ratios (E^* and S, forming the E^*/S code) to identify RNA targets with high specificity and very low false positives, a task difficult for standard hybridization techniques that are often hampered by nonspecific hybridization due to use of either multiple short probes or very long probes. The CID assay circumvents the need for complex multicolor labeling that may complicate signal interpretation due to cross-talk between overlapping emission spectra. Although the DLP capture is indirect (because it mainly depends on interactions with the transcripts rather than the capsid itself), it has the advantage of maintaining the transcriptional activity of DLPs and the structure of the exit channels. The CID assay can also be applied to other Reoviridae members, RNA viruses, and transcription systems; its applicability will also increase as single-molecule fluorescence microscopes become more robust, compact, and accessible to biology laboratories.

Channel Specialization in Rotavirus. Our CID studies of three rotavirus transcripts that differ in sequence, type of proteins

encoded, and length (S2, 2,691 nt; S6: 1,356 nt; S11: 667 nt, representing long, intermediate length, and short segments, respectively) provide unambiguous evidence that rotavirus channels specialize in extruding specific transcripts from DLPs. Our results provide direct evidence for the channel specialization model, which is also supported by the fact that ssRNA TCs are thought to form before replication within the capsid and that RNA TCs are very tightly packed within the viral particles (9, 20). Furthermore, our results, along with studies showing that RNA segments interact with unique TCs close to an exit channel (21, 22) while tightly packed in a semicrystalline state (23), preclude the possibility that extrusion of a specific transcript occurs through different channels each time.

These RNA–TC interactions, mediated through the VP1 component of TC, may guide packaging of RNA segments in the capsid; the importance of these interactions suggests that our observations on ssRNA2, ssRNA6, and ssRNA11 are likely to reflect the behavior of all rotavirus transcripts. Our results, along with structural studies, also support the suggestion that 1 of the 12 TCs is not engaged with an RNA segment.

Our results also agree with the capsid organization suggested in studies of bluetongue virus (24), another member of the Reoviridae family, which showed that the virus recruits a complete set of 10 RNA segments in the infectious capsid; notably, the absence of even a single ssRNA abrogated recruitment of the segments in the inner layered particle. The same report also suggested a hierarchy in the uncapped ssRNAs that leads to the formation of an RNA scaffold with a conserved set of RNA molecules per capsid. Although the mechanism by which rotavirus packages exactly 11 segments is not understood, it is thought that *cis*-acting sequences in the transcripts drive this process (7), as shown in influenza virus, which has eight negative-strand ssRNA segments and where it was shown (using FISH) that there is selective packaging driven by *cis*-acting regions located at the segment termini (25). In rotavirus, in silico modeling revealed the presence of regions with codon conservation that may act as structural motifs of *cis*-acting sequences (26). RNA sequences within viral segments are predicted to form conserved long-range interactions, stem loops, and codon conservation, but also dynamic ssRNA structures that may form intermolecular interactions or bind proteins to accommodate the segments in the confined space of the capsid. Under our experimental conditions, no evidence of such a scaffold was observed for total ssRNA (although we cannot discard the possibility of smaller oligomeric subunits). One possibility is that the assembly requires different reaction conditions. For example, our experiments were performed in the absence of ancillary proteins present in the DLP that may stabilize or unveil cryptic binding sites in the ssRNAs. Furthermore, the low ssRNA concentration used might have been unable to drive the formation of RNA–RNA interactions that can take place in the viroplasm (where the local RNA concentration may be very high). Further insight on the assortment process should arise from future studies on the RNA sequence, structures, or interactions that drive oligomerization; such studies will no doubt benefit from the CID assay.

Materials and Methods

Standard techniques for DNA labeling, synthesis of RNA transcripts, and DLP purification were used and are described in detail in *SI Materials and Methods*. The capture of transcripts in solution and extruded on the DLPs is described in *SI Materials and Methods*. Single molecule experiments are described in *SI Materials and Methods*. Details and procedures for data analysis are also presented in *SI Materials and Methods*.

ACKNOWLEDGMENTS. J.P. was funded by a UK Medical Research Council studentship. J.N.M.P. was funded by a UK Engineering and Physical Sciences Research Council studentship through the Oxford Doctoral Training Center at the Life Sciences Interface. C.C. and P.R. were funded by the Wellcome Trust (WT093007). A.N.K. was supported by the European Commission Seventh Framework Program (Grant FP7/2007-2013 HEALTH-F4-2008-201418), the UK Biotechnology and Biological Research Council (Grant BB/H01795X/1), and the European Research Council (Starter Grant 261227).

1. Lawton JA, Estes MK, Prasad BV (2000) Mechanism of genome transcription in segmented dsRNA viruses. *Adv Virus Res* 55:185–229.
2. Tate JE, et al.; WHO-coordinated Global Rotavirus Surveillance Network (2012) 2008 estimate of worldwide rotavirus-associated mortality in children younger than 5 years before the introduction of universal rotavirus vaccination programmes: A systematic review and meta-analysis. *Lancet Infect Dis* 12(2):136–141.
3. Trask SD, McDonald SM, Patton JT (2012) Structural insights into the coupling of virion assembly and rotavirus replication. *Nat Rev Microbiol* 10(3):165–177.
4. Mathieu M, et al. (2001) Atomic structure of the major capsid protein of rotavirus: Implications for the architecture of the virion. *EMBO J* 20(7):1485–1497.
5. Chen D, Luongo CL, Nibert ML, Patton JT (1999) Rotavirus open cores catalyze 5′-capping and methylation of exogenous RNA: Evidence that VP3 is a methyltransferase. *Virology* 265(1):120–130.
6. Prasad BV, et al. (1996) Visualization of ordered genomic RNA and localization of transcriptional complexes in rotavirus. *Nature* 382(6590):471–473.
7. Trask SD, Ogden KM, Patton JT (2012) Interactions among capsid proteins orchestrate rotavirus particle functions. *Curr Opin Virol* 2(4):373–379.
8. Settembre EC, Chen JZ, Dormitzer PR, Grigorieff N, Harrison SC (2011) Atomic model of an infectious rotavirus particle. *EMBO J* 30(2):408–416.
9. Estrozi LF, et al. (2013) Location of the dsRNA-dependent polymerase, VP1, in rotavirus particles. *J Mol Biol* 425(1):124–132.
10. Jayaram H, Estes MK, Prasad BV (2004) Emerging themes in rotavirus cell entry, genome organization, transcription and replication. *Virus Res* 101(1):67–81.
11. Johnson MA, McCrae MA (1989) Molecular biology of rotaviruses. VIII. Quantitative analysis of regulation of gene expression during virus replication. *J Virol* 63(5):2048–2055.
12. Lawton JA, Estes MK, Prasad BV (1997) Three-dimensional visualization of mRNA release from actively transcribing rotavirus particles. *Nat Struct Biol* 4(2):118–121.
13. Guglielmi KM, McDonald SM, Patton JT (2010) Mechanism of intraparticle synthesis of the rotavirus double-stranded RNA genome. *J Biol Chem* 285(24):18123–18128.
14. Kapanidis AN, et al. (2004) Fluorescence-aided molecule sorting: Analysis of structure and interactions by alternating-laser excitation of single molecules. *Proc Natl Acad Sci USA* 101(24):8936–8941.
15. Kapanidis AN, et al. (2005) Alternating-laser excitation of single molecules. *Acc Chem Res* 38(7):523–533.
16. Axelrod D (2001) Total internal reflection fluorescence microscopy in cell biology. *Traffic* 2(11):764–774.
17. Lawton JA, Estes MK, Prasad BV (1999) Comparative structural analysis of transcriptionally competent and incompetent rotavirus-antibody complexes. *Proc Natl Acad Sci USA* 96(10):5428–5433.
18. Thouvenin E, et al. (2001) Antibody inhibition of the transcriptase activity of the rotavirus DLP: A structural view. *J Mol Biol* 307(1):161–172.
19. Mason BB, Graham DY, Estes MK (1980) In vitro transcription and translation of simian rotavirus SA11 gene products. *J Virol* 33(3):1111–1121.
20. Pesavento JB, Lawton JA, Estes ME, Venkataram Prasad BV (2001) The reversible condensation and expansion of the rotavirus genome. *Proc Natl Acad Sci USA* 98(4):1381–1386.
21. McClain B, Settembre E, Temple BR, Bellamy AR, Harrison SC (2010) X-ray crystal structure of the rotavirus inner capsid particle at 3.8 A resolution. *J Mol Biol* 397(2):587–599.
22. Harvey JD, Bellamy AR, Earnshaw WC, Schutt C (1981) Biophysical studies of reovirus type 3. IV. Low-angle x-ray diffraction studies. *Virology* 112(1):240–249.
23. Gouet P, et al. (1999) The highly ordered double-stranded RNA genome of bluetongue virus revealed by crystallography. *Cell* 97(4):481–490.
24. Lourenco S, Roy P (2011) In vitro reconstitution of Bluetongue virus infectious cores. *Proc Natl Acad Sci USA* 108(33):13746–13751.
25. Chou YY, et al. (2012) One influenza virus particle packages eight unique viral RNAs as shown by FISH analysis. *Proc Natl Acad Sci USA* 109(23):9101–9106.
26. Li W, et al. (2010) Genomic analysis of codon, sequence and structural conservation with selective biochemical-structure mapping reveals highly conserved and dynamic structures in rotavirus RNAs with potential cis-acting functions. *Nucleic Acids Res* 38(21):7718–7735.

Supporting information

Periz et al. 10.1073/pnas.1220345110

SI Materials and Methods

DNA Design and Labeling. Oligonucleotides were designed using a positive-strand *segments 2, 6, or 11* as a template with amino-C6-dT modifications at the 5′ end. The Förster resonance energy transfer (FRET) efficiency E^* value of ∼0.35 was calculated using the Förster radius of the donor–acceptor pair (1) and the donor–acceptor separation (19–20 bp, ∼6.75–7.02 nm) on hybridization to the targeted transcript. The probes were relatively short (∼40 and ∼20 nt for the capture and FRET probes, respectively) to minimize formation of secondary structures, duplexes, or nonspecific binding, but still generate the required proximity. The probes targeted regions close to the 5′ end of single-stranded RNA (ssRNA) of *segments 2, 6, or 11* (ssRNA2, ssRNA6, and ssRNA11, respectively) while avoiding the conserved consensus sequence in the 5′ UTRs that may serve as assortment signals (2).

The sequence and modifications are in Table S1. Oligos T_2, T_6, T_{11}, $T_{6–11}$, T_{11}^{th}, C_2, C_6, and C_{10} were purchased as biotinylated forms (IBA), whereas C_{11} was biotinylated using sulfo-LC NHS biotin (Invitrogen). The other oligos were labeled at the 5′ end with either Cy3B or ATTO647N *N*-hydroxy-succinimidyl esters and purified using denaturing PAGE. Positive controls T_6-G_6-R_6, T_{11}-G_{11}-R_{11},$T_{(6-11)}$-G_6-R_{11} and G_{11}-Sp-R_{11}-R_{11}-$T(_{11}^{th})$ were prepared by mixing equimolar concentrations of oligos. For example T_{11}-G_{11}-R_{11} consisted of oligos T_{11}, G_{11}, and R_{11}. The annealing buffer consisted of 20 mM Tris, pH 8, 250 mM NaCl, and 1 mM EDTA. The oligo mixture was heated at 95 °C and left to cool slowly to 4 °C.

Synthetic RNA Control: T7 Synthetic Rhesus Monkey Rotavirus 11 Segment. cDNA copies of rhesus monkey rotavirus (RRV) 11 genomic segment were amplified from viral double-stranded RNA (dsRNA) in a sequence-independent manner using the method of full-length amplification of cDNAs (FLAC) (3, 4). Hairpin anchor primer C9 was ligated to viral dsRNA, followed by cDNA synthesis from gel-purified genome segments with RevertAid Premium reverse transcriptase (Fermentas) at a concentration of 10 U/μL and 55 °C for 1.5 h. PCR amplification was performed using FLAC 2 primer with KOD Hot Start DNA Polymerase (Novagen). PCR products were cloned and fully sequenced, and the T7 promoter and a suitable restriction site at the end were introduced to generate correct ends. Transcripts with a 5′-cap analog were generated from the digested T7 plasmid clones using a mMESSAGE mMACHINE T7 Ultra Kit (Ambion). Purified ssRNA were resuspended in nuclease-free water and stored at −80 °C.

Double-Layered Particle Purification. RRVs were kindly provided by H. Greenberg (Stanford, CA), and the double-layered particles (DLPs) were purified from rotavirus-infected cells as described (5). MA104 cells infected with RRV were harvested at 100% cytopathic effect; we used a multiplicity of infection (MOI) of 0.5–1 for growing stock viruses (propagation of the virus) and MOI of 3 for infection and purification of DLPs. Cells were disrupted by freezing and thawing twice, and EDTA (10 mM, pH 8) was added, followed by incubation for 1 h at 37 °C. After centrifugation, the pellet was resuspended in TNC buffer (10 mM Tris·HCl, pH 7.4, 140 mM NaCl, 10 mM $CaCl_2$) with 0.1% Nonidet P-40 and 50 mM EDTA, pH 8.0. Half volume of trichlorotrifluoethane was added to the lysate and mixed with vortex. The aqueous phase was separated by centrifugation, and DLPs were isolated by equilibrium ultracentrifugation at 100,000 × *g* in CsCl gradient for 18 h; the DLPs band was collected, diluted with TNC buffer, and pelleted by ultracentrifugation at 110,000 × *g* for 2 h.

Capture Assay of Transcripts in Solution. T7-derived positive-sense ssRNA11 (10 nM) was mixed with a hybridization buffer (100 mM Tris, pH 8.0, 9 mM $MgCl_2$, 150 mM NaCl, 0.5 U/μL RNase inhibitor), a FRET code that consisted of 10 nM each of G_{11} and R_{11} probes, and 10 nM capture probe C_{11}. The mixture was incubated for 1 h at 37 °C, and then aliquots were transferred to a total internal reflection fluorescence (TIRF)-alternating laser excitation (ALEX) microscope for analysis. The same hybridization method was performed for T7-derived positive sense ssRNA2, but using G_2 and R_2 FRET probes and capture probe C_2.

Transcription activity assays (5, 6) of DLPs were performed as above with the following modifications: DLPs (2 nM) were mixed with 20 nM of probes C6, G6, and R6. The sample was mixed in a transcription buffer of 100 mM Tris, pH 8.0, 4 mM ATP, 2 mM GTP, 2 mM CTP, 2 mM UTP, 9 mM $MgCl_2$, 150 mM NaCl, 0.5 mM S-adenosyl methionine (SAM), and 0.5 U/μL RNase inhibitor for 2 min at 37 °C, after which 2 mM EDTA was added to the reaction. Twenty-microliter aliquots were removed at time intervals of ∼1, 15, 30, 60, or 90 min, added to a slide for 2 min, and imaged using a PBS buffer with 1 mM 6-hydroxy-2,5,7,8-tetramethyl-chroman-2-carboxylic acid (TROLOX) (7) and an oxygen scavenger system (see sample preparation for details). The negative control consisted of an experiment in a transcription buffer but without nucleotides. The same hybridization method was implemented to capture ssRNA2 and ssRNA11 in solution but using specific FRET and capture probes for each transcript.

Capture Assay of Extruded Transcripts from DLPs. A suspension of DLPs in Tris, pH 8, was exchanged in PBS buffer using a Micro Bio-Spin 6 column (Bio-Rad). After that, 50 μL DLPs (2 nM) was mixed with the transcription buffer (50 mM phosphate buffer, pH 7.4, 1.4 mM KCl, 150 mM NaCl, 4 mM ATP, 2 mM GTP, 2 mM CTP, 2 mM UTP, 9 mM $MgCl_2$, 0.5 mM SAM, 0.5 U/μl RNase inhibitor) and incubated for 1 min at 37 °C. The transcription was stopped by fixing the DLPs with acidified glutaraldehyde (GT) vapor for 5 min at room temperature (8), followed by 5-min incubation with 150 mM Tris (pH 8.0) to quench the fixation reaction. The GT-containing buffer was then exchanged using a Micro Bio-Spin 6 column equilibrated in SSC buffer.

Hybridization to target ssRNAs templates was performed using a hybridization buffer, and conditions have been reported previously (9), but with several modifications. DLPs were mixed with 10 nM of C_6, G_{11}, and R_{11} and hybridization buffer consisting of 2× SSC, 9 mM citric acid (pH 6.0), 0.1% Tween-20, and 50 μg/mL heparin for 2 h at 50 °C. The hybridization buffer was then exchanged in SSC using a Micro Bio-Spin 6 column (Bio-Rad).

Capture was also performed to identify transcripts from *segment 6*; in this experiment, gentler hybridization conditions were introduced. Transcription was performed using the same buffer conditions optimized to capture segments in solution, but decreasing the concentration of nucleotides (1 mM ATP, 500 μM UTP, 500 μM GTP, 500 μM CTP). The reaction mixture was incubated for 2 min, and the reaction was then blocked using 4 mM EDTA. Probes G_6, R_6, C_{10}, and C_{11} (20 nM) were used, and the hybridization lasted for 1 h at 37 °C. Experiments were also performed to identify transcripts from *segment 2* using the

same conditions and probes G_2, R_2, C_6, and C_{11}. For the colocalization of *segments 6 and 11*, the experiment was performed as described above, but using capture probes C_6 and C_{11} and reporter probes G_6 and R_{11}. In colocalization experiments using RNA as a template, we synthesized the RNA using the same transcription conditions used in DLP capture experiments. The ssRNA was separated from the DLPs by 50-min centrifugation at 100,000 × *g* in an ultracentrifuge (rotor TLA 100.2, Optima TL; Beckman).

Capture of DLPs Bearing Extruded Transcripts Using Capture Antibodies. The experiment was performed as described previously (10) with some modifications. DLPs were allowed to transcribe for 2 min and fixed with 2% (wt/vol) paraformaldehyde for 5 min. DLPs were buffer-exchanged to SSC buffer using a micro Bio-Spin column (Bio-Rad) and interrogated using 20 nM of G_2 and R_2 FRET probes [which target (+)ssRNA2] for 2 h at 37 °C. DLPs were then buffer-exchanged in 10 mM Tris, pH 8, and 50 mM NaCl and incubated for 1 h with 66 nM sheep anti-VP6 (primary antibody ab35417; abCAM). Next, the DLPs were added for 5 min to a coverslip coated with biotinylated rabbit anti-sheep secondary antibody (ab6746; abCAM), prepared by incubating the coverslip with secondary antibody (26 nM in the same buffer conditions) for 30 min followed by a PBS wash. We used two negative controls to test nonspecific interactions of antibodies to DLPs: the first had the primary antibody substituted by rabbit γ-globulins (purified from nonimmunized rabbit serum, 011-000-002; Jackson ImmunoResearch), and the second was performed in the absence of biotinylated secondary antibody.

Sample Preparation. Biotinylated DNA constructs were bound to neutravidin-coated glass coverslides (11). These coverslides were prepared in the following way. Silicone gaskets (Grace Bio-Labs) were placed onto a neutravidin-treated coverslip, and a second coverslip used to seal the imaging chambers from oxygen. Imaging buffers were used in buffer PBS (pH 7.4). All imaging buffers contained an enzymatic oxygen scavenging system [10% (wt/vol) glucose, 1 mg/mL glucose oxidase, and 40 μg/mL catalase]. The imaging buffer contained 1 mM TROLOX.

ALEX Microscopy. Samples were imaged on a custom-built TIRF microscope, using ALEX (12). The red laser (635 nm, Cube model; Coherent) was directly modulated, and the green laser (532 nm, continuous wave, Samba model; Cobolt) was modulated with acousto-optical modulator (AA optics) with an alternation period of 100 ms. Because the imaging was performed using TIRF microscopy, which mainly detects signals within an evanescent field of ∼100 nm, the assay reflects mainly the fluorescence of surface-captured molecules or particles.

Laser beams were coupled into a single-mode optical fiber, and output from the fiber was collimated and directed into an inverted microscope IX71 Olympus through a 100× oil immersion Olympus objective, numerical aperture (NA) 1.4. The fluorescence emission is collected by the same objective and separated from the excitation path by a dichroic mirror (545/650 nm; Semrock) and additional filters (545 nm LP, Chroma; 632/25 nm notch filter; Semrock). Dual-color detection is achieved by splitting the emission light into red and green channels (630 DRLP; OMEGA) and projecting onto two regions of an EMCCD camera (iXon+; Andor). The intensities of the lasers were measured before the entry into the TIRF objective and were set to 1.5 (635 nm) and 0.75 mW (532 nm) for Cy3B and ATTO647N, respectively. Because the relative probe stoichiometry S signal depends on the relative brightness of the fluorophore, the laser powers were chosen to yield a value of $S \sim 0.5$ for a stoichiometry of 1:1 for the Cy3B–ATTO647N pair used in the FRET probes and the positive controls.

We note that 12.5% of the intensity detected in the green channel leaks into the red channel, which generates an apparent FRET baseline of $E^* = 0.11$ from a Cy3B-only signal. This FRET baseline is due to the imperfect color splitting and the natural spectral leakage of Cy3B into the red channel. The red channel intensity of ATTO647N when excited by the 532-nm laser is 3% of the intensity of Cy3B excited by the 532-nm laser (or ATTO647N excited by the 635-nm laser). Therefore, the apparent FRET is $E^* = 0.13$ when both donor and acceptor are present without actual FRET.

Data Analysis. Data analysis was performed as described (13). Briefly, the extraction of each single-molecule intensity trajectory was analyzed with custom software written in MATLAB (MathWorks) (13). The alignment of the green and red channels is performed with a peak-finding algorithm, and the emission intensities are filtered using ellipticity and nearest neighbor criteria ($\varepsilon < 0.7$, $NN > 5$ pixels) to eliminate colocalization artifacts due to the overlapping of two close point spread functions (PSFs). Three emission intensities are recorded from ALEX data: F_{DD} is the fluorescence intensity resulting from the donor emission on donor excitation; F_{DA} is the fluorescence intensity resulting from the donor emission on acceptor excitation; and F_{AA} (or $A_{ex}A_{em}$) is the fluorescence intensity resulting from the acceptor emission on acceptor excitation. These intensities are estimated by fitting a 2D Gaussian to each PSF. The apparent FRET efficiency, E^*, and relative fluorophore stoichiometry, S, were calculated by

$$E^* = \frac{F_{DA}}{F_{DD} + F_{DA}} \qquad S = \frac{F_{DD} + F_{DA}}{F_{DD} + F_{DA} + F_{AA}}.$$

Histograms display the combined data of movies recorded in identical conditions. Statistical analysis ANOVA (Tukey's test) and the t test were performed and plotted using GraphPad (GraphPad Software).

Correction of Nonuniform Illumination in the Field of View. In our experiments, the detected fluorescence intensity from a single molecule correlated significantly with the location of the molecule within the field of view. This correlation is mainly due to the nonuniform excitation field across the field of view, which has a profile that can be approximated by an elliptical 2D Gaussian. We have corrected for the nonuniform excitation (see $A_{ex}A_{em}$ intensity distributions in Figs. S1 and S4) as follows: for each molecule that emitted at a stable level (no photoblinking and no photobleaching), we calculated the mean intensity counts per frame $\overline{F}$ (e.g., in the acceptor channel) and localization position $(\bar{x}, \bar{y})$. A 2D Gaussian function of the form

$$f_F(x,y) = b + A \exp\left[-\frac{(x-\mu_x)^2}{2\sigma_x^2} - \frac{(y-\mu_y)^2}{2\sigma_y^2}\right] = b + A\phi(x,y)$$

was fitted to the set of experimental data points $\{\overline{F}(\bar{x},\bar{y})\}$, compiled from all single molecules detected in movies taken under identical conditions. The single-frame intensities F of a molecule found at $(\bar{x},\bar{y})$ were then corrected by

$$F^* = b + \frac{F-b}{\phi(\bar{x},\bar{y})},$$

corresponding to a mapping to a normalized intensity level $b + A$. In other words, F^* corresponds to the intensity one would observe if the position of the molecule were at (μ_x, μ_y), the maximum of the 2D Gaussian profile f_F. The corrected intensities are marked with an asterisk, i.e., $A_{ex}A_{em}{}^*$.

A single-molecule intensity time series $F = \{F_1, \ldots, F_{20}\}$ (20 × 100-ms ALEX frames) was determined to be stable if not more

than two consecutive frames showed intensity counts deviating from the median intensity more than two times the median absolute deviation (MAD)

$$\mathrm{MAD}(F) = \mathrm{Median}(\{|F_i - \mathrm{Median}(F)|\})$$

in both detection channels. MAD is a robust estimator for the SD s, and for normally distributed data, it can be shown that $\sigma \approx 1.48$ MAD.

Number of Colocalizations Observed vs. the Number Expected Due to Random Coincidence Even if the donor and acceptor particles localize independently, we still expect to detect colocalizations with our data analysis software Twotone due to the probability of probes coming closer than our colocalization search radius threshold of $R_{\mathrm{search}} = 250$ nm. A pair of donor and acceptor particles is considered as colocalized if the donor-acceptor distance is less than R_{search} and if no further donor or acceptor particles are present within a vicinity of $R_{\mathrm{exclude}} = 500$ nm from each of the particles under consideration. With the observed densities of donor and acceptor particles ρ_D and ρ_A in each field of view, the expected random colocalization density can be estimated as

$$\rho_{\mathrm{coloc}} = \pi R_{\mathrm{search}}^2 \rho_D \rho_A (1 - \pi R_{\mathrm{exclude}} \rho_D)(1 - \pi R_{\mathrm{exclude}} \rho_A).$$

This formula overestimates the number of detected random colocalizations because additional filters are in place to exclude particles with elliptical point spread functions (arising from closely spaced particles), as well as particles that fall below an intensity threshold. We determined ρ_D and ρ_A by counting the number of donor and acceptor particles in the homogenously illuminated part of the field of view and dividing by the area.

The number of observed colocalizations was tested against the number of estimated random colocalizations using a one-sided paired-sample Wilcoxon signed-rank in MATLAB (MathWorks). We used a paired test of the observed number and estimated number from the same movie, because both depend on the density of donor and acceptor signals. This test is preferable to a paired t test, as our test does not assume normally distributed data.

1. Holden SJ, et al. (2010) Defining the limits of single-molecule FRET resolution in TIRF microscopy. *Biophys J* 99(9):3102–3111.
2. McDonald SM, Patton JT (2011) Assortment and packaging of the segmented rotavirus genome. *Trends Microbiol* 19(3):136–144.
3. Boyce M, Celma CC, Roy P (2008) Development of reverse genetics systems for bluetongue virus: Recovery of infectious virus from synthetic RNA transcripts. *J Virol* 82(17):8339–8348.
4. Maan S, et al. (2007) Rapid cDNA synthesis and sequencing techniques for the genetic study of bluetongue and other dsRNA viruses. *J Virol Methods* 143(2):132–139.
5. Patton JT, Chizhikov V, Taraporewala Z, Chen D (2000) *Rotavirus, Methods and Protocols: Virus Replication*, eds Gray J, Desselberger U, (Humana, Totowa, NJ), pp 33–66.
6. Cohen J, Laporte J, Charpilienne A, Scherrer R (1979) Activation of rotavirus RNA polymerase by calcium chelation. *Arch Virol* 60(3-4):177–186.
7. Rasnik I, McKinney SA, Ha T (2006) Nonblinking and long-lasting single-molecule fluorescence imaging. *Nat Methods* 3(11):891–893.
8. Fadouloglou VE, Kokkinidis M, Glykos NM (2008) Determination of protein oligomerization state: Two approaches based on glutaraldehyde crosslinking. *Anal Biochem* 373(2):404–406.
9. Choi HM, et al. (2010) Programmable in situ amplification for multiplexed imaging of mRNA expression. *Nat Biotechnol* 28(11):1208–1212.
10. Chou YY, et al. (2012) One influenza virus particle packages eight unique viral RNAs as shown by FISH analysis. *Proc Natl Acad Sci USA* 109(23):9101–9106.
11. Roy R, Hohng S, Ha T (2008) A practical guide to single-molecule FRET. *Nature Methods* 5(6):507–516.
12. Margeat E, et al. (2006) Direct observation of abortive initiation and promoter escape within single immobilized transcription complexes. *Biophys J* 90(4):1419–1431.
13. Uphoff S, et al. (2010) Monitoring multiple distances within a single molecule using switchable FRET. *Nat Methods* 7(10):831–836.

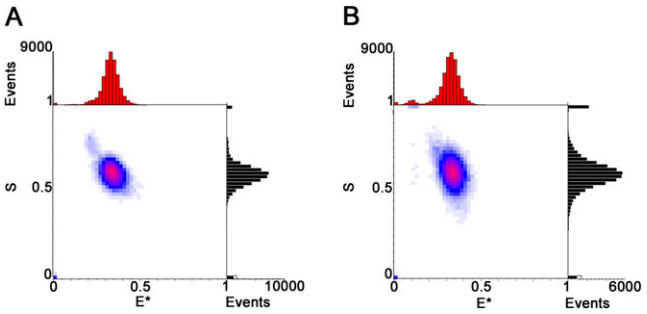

Fig. S1. The copy number of specific transcripts during their extrusion from transcriptionally active DLPs using a novel single-molecule fluorescence assay for transcript capture and identification (CID) assays for ssRNA11 and ssRNA6 transcripts produced by rotavirus DLPs. ssRNAs were incubated with capture and FRET probes, captured on the surface, and detected using ALEX-TIRF. (*A*) (+)ssRNA11 detected using G_{11} and R_{11} FRET probes and capture probe C_{11}. Combined *E*/S* histogram data of 2,553 detected particles with an *E*/S* signature of 0.35/0.55, well matching the code of 0.35/0.5. (*B*) (+)ssRNA6 detected using G_6 and R_6 FRET probes and capture probe C_6. Combined *E*/S* histogram data of 2,696 detected particles with an *E*/S* signature of 0.35/0.6, well matching the code of 0.35/0.5.

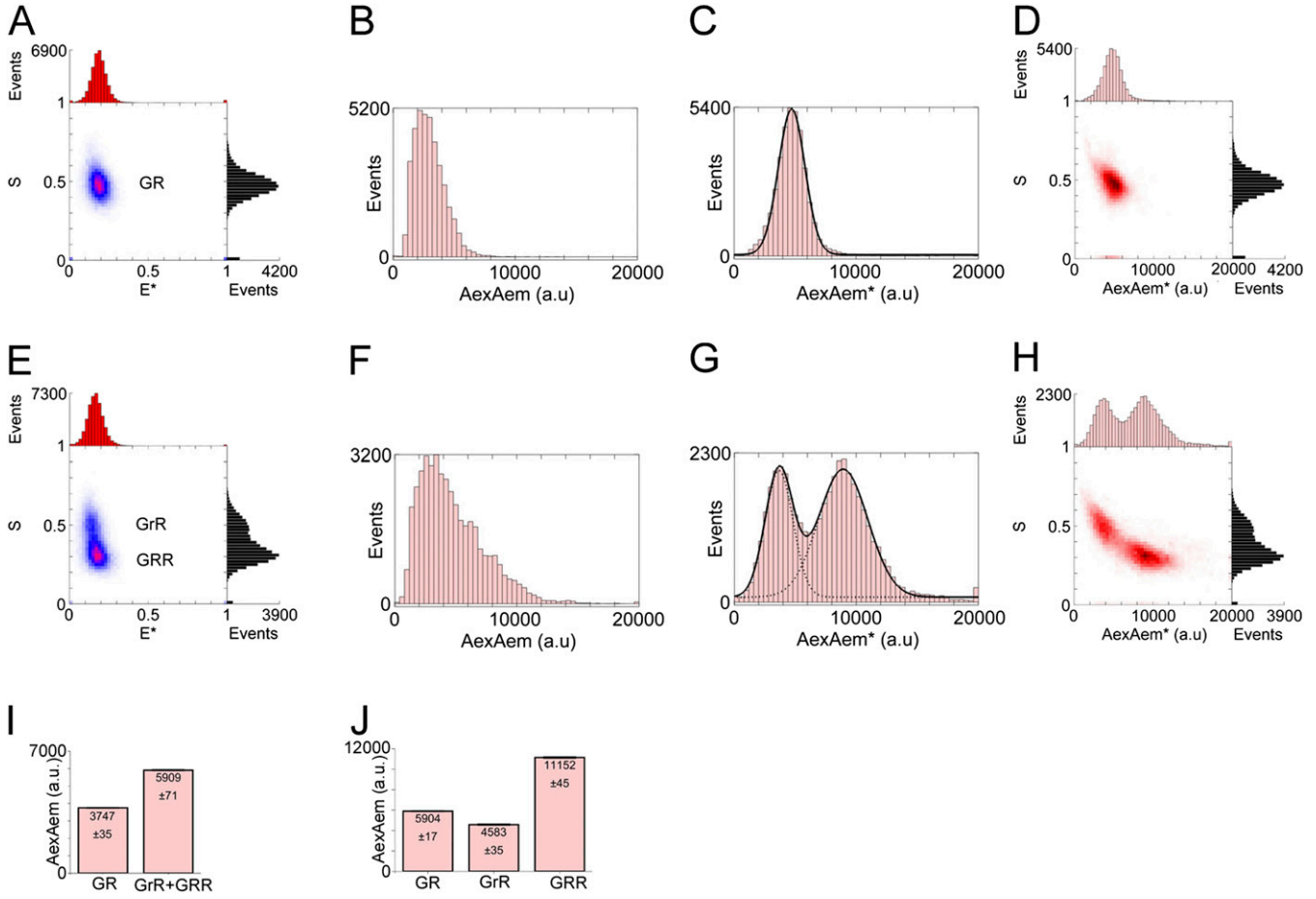

Fig. S2. Standards analyzed using *E*/S* histograms and fluorescence intensities. (*A*) *E*/S* histogram of dsDNA construct G_6-R_6-$T_{(6\text{-}11)}$ (a GR standard, meaning that the construct has one green labeled hybridized probe "G" and one red labeled hybridized probe "R"), compiled from 1,959 particles. The long fluorophore separation (40 bp) leads to negligible FRET. The population at $S \sim 0.5$ has the signal expected from constructs carrying one red and one green fluorophore. (*B*) Histogram of $A_{ex}A_{em}$ intensities for the GR standard (mean ± SEM: 3,747 ± 35 a.u.). (*C*) As in *B*, but corrected for nonuniform illumination (corrected emission intensities, $A_{ex}A_{em}$*). The fitted Gaussian function was centered at 5,904 ± 17 a.u. (*D*) $S/A_{ex}A_{em}$* histogram of the GR constructs shows that the well-defined population of $S \sim 0.5$ corresponds to a well-defined population of $A_{ex}A_{em}$* intensity centered at 5,909 a.u. (*E*) *E*/S* histogram of dsDNA construct G_{11}-Sp-R_{11}-R_{11}-$T_{(11^{th})}$ (a GRR standard, meaning that the construct has one green labeled hybridized probe "G" and two red labeled hybridized probes "R"). The long fluorophore separation (47 bp) leads to negligible FRET. The histogram (2,247 particles) shows a major population at $S \sim 0.3$ and a minor population at $S \sim 0.5$, consistent with a main population of fully hybridized constructs (GRR) and a minor population with a single R probe (GrR, meaning that the construct has one green labeled hybridized probe "G" but only one red labeled hybridized probe "R" out of the two sites available to red labeled probes; GrR is photophysically equivalent to the GR standard). (*F*) Distributions of $A_{ex}A_{em}$ intensities (5,909 ± 71 a.u.) from GRR samples, with 26% of GRR particles showing intensities >7,500 a.u. (cf. 1.5% of GR in *B*). (*G*) Distributions of $A_{ex}A_{em}$* intensities, revealing two well-resolved populations centered at 4,583 ± 35 and 11,152 ± 45 a.u., both fit to Gaussian functions. The lower intensity for GRR compared with the GR standard may indicate fluorophore interactions with the nonhybridized portion of DNA. (*H*) Two distinct $A_{ex}A_{em}$* populations can also be visualized on the S*/$A_{ex}A_{em}$* histogram. (*I* and *J*) Mean values and Gaussian fit results with error estimates.

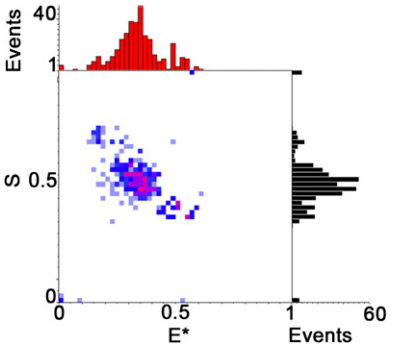

Fig. S3. Transcriptionally active DLPs carry a single extruded transcript for *segment 6*. CID of actively transcribing DLPs (allowed to transcribe for 2 min) were interrogated using capture probe C_{11} [which targets extruded (+)ssRNA11] and FRET probes G_6 and R_6 [which target extruded (+)ssRNA6]. The hybridization conditions are as described for capturing ssRNA6 using two capture probes. Combined *E*/S* histogram data of 38 detected particles show a main population centered at 0.35/0.5, which is the expected *E*/S* code for this transcript.

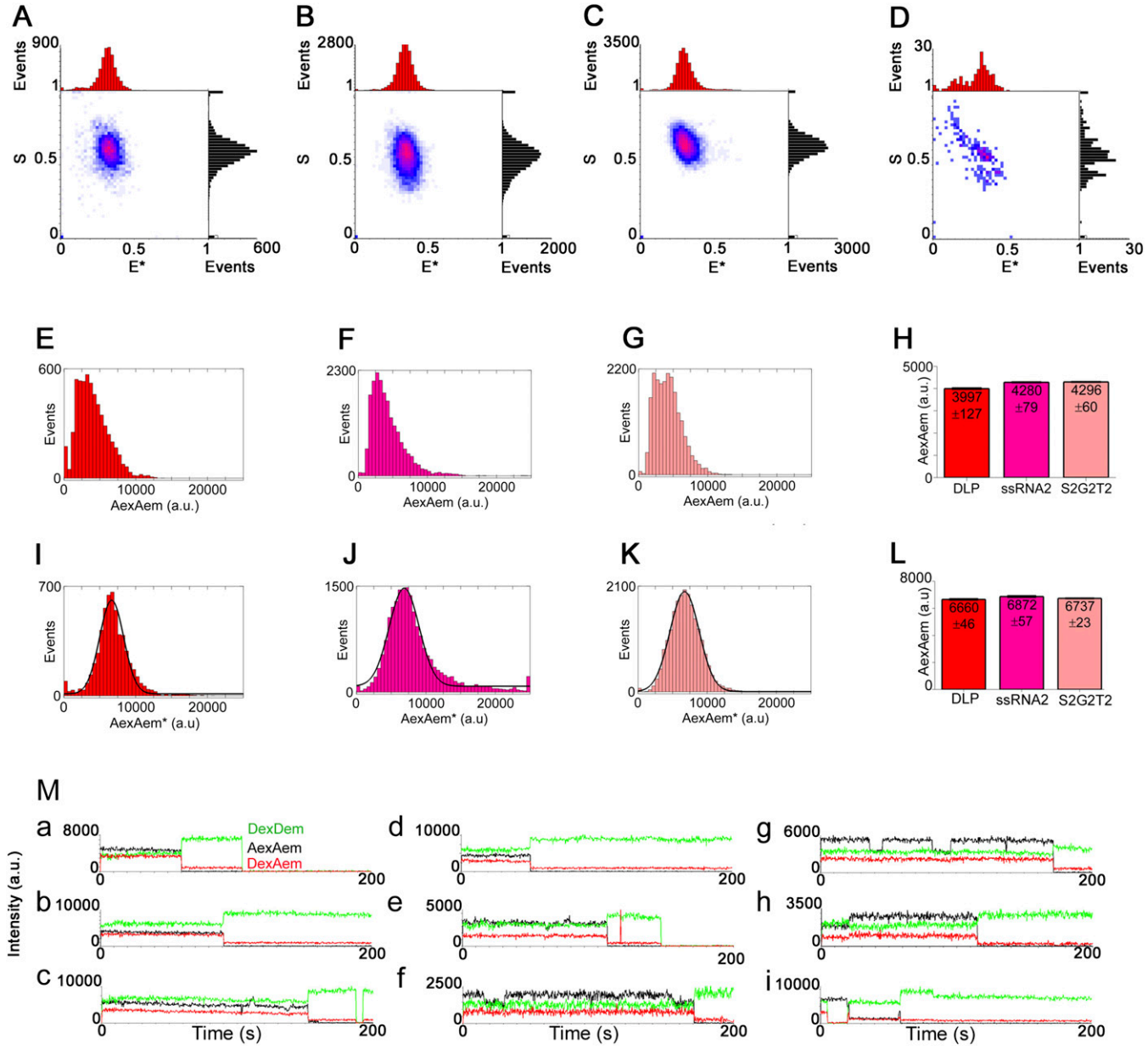

Fig. S4. Transcriptionally active DLPs carry a single extruded transcript for *segment 2*. (*A*) Actively transcribing DLPs (allowed to transcribe for 2 min) interrogated using capture probes C_6 and C_{11} and FRET probes G_2 and R_2 [which target extruded (+)ssRNA2]. The *E*/S* histogram (292 particles) shows a population of 0.35/0.5, matching the positive control (*B* and *C*). (*B*) Positive control. *E*/S* histogram (998 particles) of synthetic ssRNA2 hybridized with G_2 and R_2 and captured on the surface with capture probe C_2. (*C*) Positive control. *E*/S* histogram (1,079 particles) of G_2-R_2-T_2 dsDNA construct that consists of one G_2 and one R_2 probe hybridized to biotinylated T_2 ssDNA. (*D*) Negative control. *E*/S* histogram (11 particles) experiment performed with DLPs and FRET probes but without capture probes shows very few particles attached to the surface. (*E–G*) Distributions of average $A_{ex}A_{em}$ intensities from the sample in *A* (red), *B* (dark pink, positive control), and *C* (light pink, positive control). (*H*) Comparison of mean $A_{ex}A_{em}$ from ssRNA2 extruded in DLPs shown in *E* (red), captured ssRNA2 (*F*, dark pink, positive control), and dsDNA control (*G*, light pink). (*I–K*) Corrected $A_{ex}A_{em}$* intensity distributions from *A–C*, respectively, along with single Gaussian fits. (*L*) Mean $A_{ex}A_{em}$* intensity from the Gaussian fits for DLPs (*E*), ssRNA2 (*F*), and dsDNA control (*G*). (*M*) Photobleaching examples of DLPs captured with extruded ssRNA2 (39 particles). CID was performed as in *A* but taking longer movies (2,000 frames, 100-ms frames in *A–E* and *I* and 50-ms frames in *F–H*). Approximately 90% of the particles showed a single photobleaching step in the acceptor channel, whereas 10% displayed complex photophysics (see *I*).

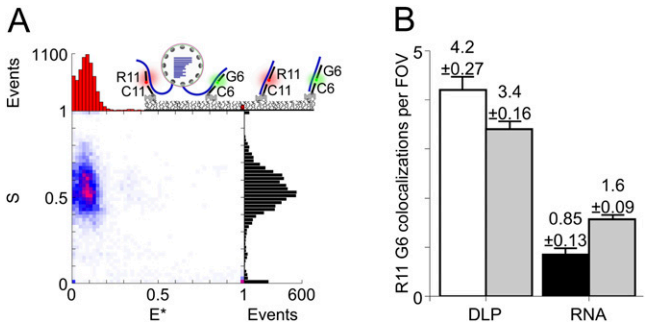

Fig. S5. Colocalization of (+)ssRNA6 and (+)ssRNA11 on DLPs. (*A*) CID of actively transcribing DLPs (allowed to transcribe for 2 min) interrogated using probes C_6 and G_6 [which target extruded (+)ssRNA6] and probes C_{11} and R_{11} [which target extruded (+)ssRNA11]. The *E*/S* histogram ($n = 357$, 80 movies) showed the expected *E*/S* value of ∼0.1/0.5, matching that of the positive control (*B*). (*B*) Comparison of the mean number of observed colocalizations per 25 × 25-μm field of view, with the mean estimated number of random colocalizations (gray columns; all error bars: SEM). For each field of view, the expected number of random colocalizations was calculated using the number of R_{11} and G_6 particles in each field of view. For the DLP experiment in *A* (white column), use of the one-sided paired-sample Wilcoxon signed-rank test showed that significantly more colocalizations were observed than expected by random colocalization ($P = 0.0004$; on average, 90 R_{11} and 183 G_6 particles). For the RNA experiment, fewer colocalizations were observed (black column; 34 colocalizations in 40 movies) than expected due to random colocalization; therefore, $P = 1$ (on average, 66 R_{11} and 98 G_6 particles per field of view). A control experiment using the same hybridization conditions as for the DLP sample but without the addition of nucleotides led to the capture of only two colocalized particles (20 movies) and no significantly higher colocalization than expected by chance ($P > 0.05$; on average, 1.8 R_{11} and 5.6 G_6 signals per field of view).

Table S1. Oligonucleotide DNA used in this study

Oligo	Segment sequence	Oligo sequence	Modification
G_6	(+17/+36)B	5′-ACAGGACATCCATGTTGAAG-3′	Cy3B 5′end
R_6	(+37/+56)B	5′-AAGAGTTTTTGACAAGGAGT-3′	ATTO647N 5′end
T_6	(+14/+56)T	5′-AGTCTTCAACATGGATGTCCTGTACTCCTTGTCAAAAA CTCTT-3′	Biotin 5′end
C_6	(+56/+95)B	5′-GTATAATGTGCCTTCGTCAATTTTGACTCTAGCATCTT TA-3′	Biotin 5′end
C_{10}	(+21/+40)B	5′-TTTCCGCACGCGCTCTCTCG-3′	Biotin 5′ end
G_{11}	(+16/+35)B	5′-ATACTGAGAGACATCACTGT-3′	Cy3B 5′end
R_{11}	(+36/+54)B	5′-TGGAAGACTTGTCACGTCA-3′	ATTO647N 5′end
T_{11}	(+15+54)T	5′-TACAGTGATGTCTCTCAGTATTGACGTGACAAGTCTTC CA-3′	Biotin 5′end
C_{11}	(+55+94)B	5′-TGAAGATGATTCATGTTTATAAATGCTGGAGGAAATA GA-3′	Biotin 5′end
$T_{(6\text{-}11)}$	Hybrid template	5′-AGTCTTCAACATGGATGTCCTGTTCC AAGTTAAGTGATCTA ATTCAACTGA CGTGACAAGTCTTCCA-3′	Biotin 5′end
$T_{(11^{th})}$	Hybrid template	5′-ACAGTGATGTCTCTCAGTATTCCAAGTTAAGTGATCTAATTCAA CTGACGTGACAAGTCTTCCATGACGTGACAAGTCTTCCA-3′	Biotin 5′end
Sp	(spacer sequence)	5′GTTGAATTAGAAGATCACTTAACTTGGA3′	
G_2	(+41+60)B	5′-TTTAAATTCGTCTCACGACG-3′	Cy3B 5′end
R_2	(+61+79)B	5′-TTGCATTCGATCATCTTGT-3′	ATTO647N 5′end
T_2	(+41+79)T	5′-CGTCGTGAGACGAATTTAAAACAAGATGATCGAATGCAA-3′	Biotin 5′end
C_2	(+21+40)B	5′-CGCTCCACGCTTTCTGTACG-3′	Biotin 5′end

Oligos are described with a capital letter that indicates the type of probe and labeling used followed by a subscript indicating the segment. The (+) ssRNA sequences are named as top strand (T) and numbered from the 5′ end (+1). Oligo sequences are designed using the (+)ssRNA as a template; B denotes bottom strand complementary to a sequence in the T strand. G is a green FRET probe labeled with Cy3B; R is a red FRET probe labeled with ATTO647N corresponding to the segment used as a template; C is a capture probe labeled with biotin. Sp is a spacer sequence based partially on a ssRNA6 genomic sequence, and is part of the long dsDNA control which consisted of one G_{11} and two R_{11} probes hybridized to complementary sequence $T(_{11}{}^{th})$. Sp minimizes the flexibility and nonspecific hybridization of probes in the G_{11}-Sp-R_{11}-R_{11}-$T(_{11}{}^{th})$ construct.